Nuclear Energy in Central Europe '98
Terme Čatež, September 7 to 10, 1998

ESE a 2D Compressible Multiphase Flow Code Developed for MFCI Analysis – Code Validation

Matjaž Leskovar, Borut Mavko
"Jožef Stefan" Institute
Jamova 39, 1000 Ljubljana, Slovenia
E-mail: matjaz.leskovar@ijs.si, http://www2.ijs.si/~mleskovar/

ABSTRACT – ESE (Evaluation of Steam Explosions) is a general second order accurate two-dimensional compressible multiphase flow computer code. It has been developed to model the interaction of molten core debris with water during the first premixing stage of a steam explosion. A steam explosion is a physical event, which may occur during a severe reactor accident following core meltdown when the molten fuel comes into contact with the coolant water. Since the interfacial exchanges of mass, momentum and energy are regime dependent, different exchange laws have been incorporated in ESE for the major flow regimes.

With ESE a number of premixing experiments performed at the Oxford University and at the QUEOS facility at Forschungszentrum Karlsruhe has been simulated. In these premixing experiments different jets of spheres were injected in a water pool. The ESE validation plan was carefully chosen, starting from very simple, well-defined problems, and gradually working up to more complicated ones.

The results of ESE simulations, which were compared to experimental data and also to first order accurate calculations, are presented in form of graphs. Most of the ESE results agree qualitatively as quantitatively reasonably well with experimental data and they are in general better than the results obtained with the first order accurate calculation.

Nomenclature

c_p	specific heat at constant pressure
C	drag coefficient
D	length scale (diameter)
f	function
$\vec{\mathbf{F}}$	interfacial force
h	heat transfer coefficient
n	number of drops per unit volume
Pr	Prandtl number
q_{wv}	enthalpy of evaporation
$\dot{Q}$	interfacial heat transfer
Re	Reynolds number
T	temperature
$\vec{\mathbf{v}}$	velocity
We_{cr}	critical Weber number for bubble/drop breakup

Greek Letters

α	phase presence probability
ε	emissivity
ϕ	area concentration factor
γ	surface tension
λ	thermal conductivity
μ	dynamic viscosity
ϑ	phase presence probability fraction
ρ	density
σ	Stefan-Boltzmann coefficient

Subscripts / Superscripts

c,d	continuous, dispersed
f,w,v	fuel, water, vapor phase
$lam,turb$	laminar, turbulent
r,c	radiation, convection
s	saturation
vm,l	virtual mass, lift force

1. Introduction

The ESE (Evaluation of Steam Explosions) computer code has been developed to model the interaction of molten core debris with water during the first premixing stage of a steam explosion [1]. A steam explosion is a physical event, which may occur during a severe reactor accident following core meltdown when the molten fuel comes into contact with the coolant water.

ESE is a general second order accurate two-dimensional compressible multiphase flow computer code. It takes into account the violent steam generation when melt pours into water, the thermal-hydraulic interaction between the melt, water, steam and air phases, and the resulting fragmentation and cooling of the melt. Since the interfacial exchanges of mass, momentum and energy are regime dependent, different exchange laws, which were taken mainly from the PM-ALPHA computer code [2], have been incorporated in ESE for the major flow regimes. The flow regimes considered in characterizing interface transfers are bubbly flow, churn-turbulent flow, droplet flow and flow through a porous bed of fuel particles. These flow regimes are identified by simple phase probability criteria. In the calculation of interfacial momentum coupling and interfacial heat transfer special phenomena like the added mass effect, lift forces and radiation are also considered.

With ESE a number of premixing experiments performed at the Oxford University [3] and at the QUEOS facility [4] at Forschungszentrum Karlsruhe has been simulated. In these premixing experiments different jets of spheres were injected in a water pool. The sphere properties like density, size, temperature, impact velocity and also the number of spheres were systematically changed between these experiments. The ESE validation plan was carefully chosen, starting from very simple, well-defined problems, and gradually working up to more complicated ones. The hydrodynamic part of ESE could be tested separately using results from the Gilbertson experiments performed in rectangular geometry and the isothermal QUEOS experiments performed in axial-symmetric cylindrical geometry. The complete behavior of ESE was validated using results from the hot integral QUEOS experiments. To get a better understanding of ESE's numerical behavior all calculations were performed, beside using ESE's second order accurate high-resolution method, also using a first order accurate upwind method and a convergence analysis has been done.

2. The Exchange Laws

The interfacial exchanges of mass, momentum and energy are clearly regime dependent, and uncertainties remain even for two-phase flows. For now, our approach aims to incorporate first-order physics that accounts for the major flow and heat transfer regimes as identified by simple criteria of fuel presence probability α_f and vapor presence probability fraction $\vartheta_v = \alpha_v/(\alpha_v + \alpha_w)$. The flow regimes are shown in Fig.1. For $\alpha_f < 0.3$ we consider the fuel particles immersed in a two-phase gas-liquid flow, whose own flow regimes are defined by the value of the vapor presence probability fraction: $\vartheta_v \le 0.3$ (bubbly), $0.3 < \vartheta_v < 0.7$ (churn-turbulent), and $\vartheta_v \ge 0.7$ (droplet). For $\alpha_f \ge 0.3$, as the fuel particles are densely packed, we consider a flow of gas and liquid through a porous bed of fuel particles.

We use the exchange laws available for two-phase systems after making suitable modifications to account for, as a first approximation, the effect of a third phase. In calculating interfacial momentum exchange, one needs to know the projected area concentration of the dispersed phase. Also, in calculating interfacial heat exchange, one needs to know the interfacial area concentration. In a two-phase system, these area concentrations

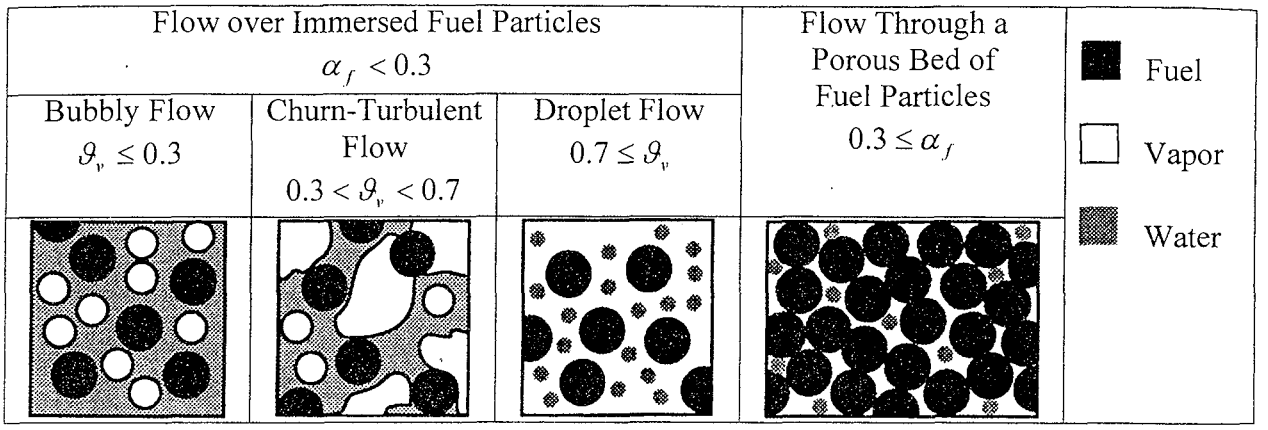

Figure 1: Schematic diagram of flow regimes considered in characterising interface transfers.

can be estimated from the length scale and the presence probability of the dispersed phase. However, the presence of a third phase reduces the area concentration as the third phase must also share the same area. Therefore, we modify the area concentration by a factor $\phi_{ij} = \alpha_j / (\alpha_j + \alpha_k)$, which represents the effect of the phase k on the area concentration of phase i for its interaction with phase j.

2.1 Interfacial momentum coupling

The interfacial momentum coupling is primarily due to drag. For the bubbly flow regime ($\vartheta_v \le 0.3$) we have also included the added mass effect

$$\vec{\mathbf{F}}_d^{vm} = 0.5\alpha_d \rho_c \phi_{dc} \left(\frac{D_c \vec{\mathbf{v}}_c}{Dt} - \frac{D_d \vec{\mathbf{v}}_d}{Dt} \right) \tag{1}$$

and lift forces

$$\vec{\mathbf{F}}_d^{l} = 0.5\alpha_d \rho_c \phi_{dc} (\vec{\mathbf{v}}_c - \vec{\mathbf{v}}_d) \times (\nabla \times \vec{\mathbf{v}}_c). \tag{2}$$

For $\alpha_f < 0.3$ the drag force is calculated from

$$\vec{\mathbf{F}}_d = \frac{3}{4}\alpha_d \rho_c \phi_{dc} \frac{C}{D_d} |\vec{\mathbf{v}}_c - \vec{\mathbf{v}}_d| (\vec{\mathbf{v}}_c - \vec{\mathbf{v}}_d), \tag{3}$$

where the drag coefficient for churn flow ($0.3 < \vartheta_v < 0.7$) is defined by

$$d = v, c = w, C = \frac{8}{3}(1 - \vartheta_v) \tag{4}$$

and for dispersed flow by

$$\left.\begin{array}{lll} \vartheta_v \le 0.3, & d = v, c = w, & f = (1-\vartheta_v)^{1.5} \\ \vartheta_v \ge 0.7, & d = w, c = v, & f = \vartheta_v^{\,3} \\ & d = f, c = \{w, v\}, & f = (1-\alpha_f)^{1.5} \end{array}\right\} \quad C = 0.45 \left(\frac{1 + 17.67 f^{6/7}}{18.67 f} \right)^2. \tag{5}$$

The length scale (diameter) D_d is obtained from

$$\frac{\rho_c |\vec{\mathbf{v}}_c - \vec{\mathbf{v}}_d|^2 D_d}{\gamma} = \mathrm{We}_{cr} \begin{cases} 8 & d = v \\ 12 & d = w \end{cases}. \tag{6}$$

For the "dense fuel regime" ($\alpha_f \ge 0.3$) we use laminar and turbulent permeabilities (7)

$$\vec{\mathbf{F}}_{df} = \vec{\mathbf{F}}_{df}^{lam} + \vec{\mathbf{F}}_{df}^{turb}, d = \{v, w\},$$

where

$$\vec{\mathbf{F}}_{df}^{lam} = \begin{cases} 150\dfrac{\alpha_d \alpha_f^2}{(1-\alpha_f)^3}\dfrac{\mu_d}{D_f^2}\left(\vec{\mathbf{v}}_d - \vec{\mathbf{v}}_f\right), & \mathrm{Re}'_d < 1000 \\ 0, & \mathrm{Re}'_d \geq 1000 \end{cases} \tag{8}$$

and

$$\vec{\mathbf{F}}_{df}^{turb} = \begin{cases} 1.75\dfrac{\alpha_d \alpha_f}{(1-\alpha_f)^3}\dfrac{\alpha_d \rho_d \left|\vec{\mathbf{v}}_d - \vec{\mathbf{v}}_f\right|}{D_f}\left(\vec{\mathbf{v}}_d - \vec{\mathbf{v}}_f\right), & \mathrm{Re}'_d > 10 \\ 0, & \mathrm{Re}'_d \leq 10 \end{cases} \tag{9}$$

with

$$\mathrm{Re}'_d = \alpha_f \frac{\alpha_d \rho_d D_f \left|\vec{\mathbf{v}}_d - \vec{\mathbf{v}}_f\right|}{\mu_d}. \tag{10}$$

2.2 Interfacial heat transfer

The distinction of the fuel-to-coolant heat transfer mechanisms is made again on the basis of the flow regimes. The key distinction is whether or not there is sufficient water in the coolant phase to completely engulf the fuel particles, thus a vapor presence probability fraction criterion is used.

For $\vartheta_v < 0.7$, heat transfer to water is estimated by superposition of radiation and film boiling heat fluxes

$$\begin{aligned} \dot{Q}_{fw} &= n_f \left(h_r + h_c\right)\pi D_f^2 \phi_{fw}\left(T_f - T_w\right), \; n_f = \frac{6\alpha_f}{\pi D_f^3}, \\ h_r &= \sigma \varepsilon_f \frac{T_f^4 - T_w^4}{T_f - T_w}, \; h_c = 2.98\left(\frac{\rho_v \lambda_v \left(q_{ww} + 0.68 c_{pv}\left(T_f - T_w\right)\right)}{D_f\left(T_f - T_w\right)}\right)^{1/2}. \end{aligned} \tag{11}$$

The emissivity value $\varepsilon_f = 0.7$ is selected for the calculations of typical interest. Heat transfer from fuel to vapor in this regime need not to be accounted for separately.

For $\vartheta_v \geq 0.7$, we assume a vapor-continuous regime in which heat is transferred to liquid drops by irradiation and to the gas by convection. The gas is allowed to superheat and convert heat to the liquid drops, which boil at saturation. Thus

$$\begin{aligned} \dot{Q}_{fw} &= \min\left(n_w \pi D_w^2, n_f \pi D_f^2\right)\sigma \varepsilon_f \varepsilon_w \left(T_f^4 - T_w^4\right), \\ \dot{Q}_{fv} &= n_f \phi_{fv} \pi D_f^2 h'_c \left(T_f - T_v\right), \; n_w = \frac{6\alpha_w}{\pi D_w^3}, \end{aligned} \tag{12}$$

where for $\alpha_f < 0.3$

$$h'_c = \frac{\lambda_v}{D_f}\left(2 + 0.6\,\mathrm{Re}_v^{1/2}\,\mathrm{Pr}_v^{1/3}\right), \; \mathrm{Re}_v = \frac{\rho_v \left|\vec{\mathbf{v}}_v - \vec{\mathbf{v}}_f\right| D_f}{\mu_v}, \; \mathrm{Pr}_v = \frac{\mu_v c_{pv}}{\lambda_v} \tag{13}$$

and for $\alpha_f \geq 0.3$

$$\begin{aligned} h'_c &= 0.91 c_{pf} \alpha_v \rho_v \left|\vec{\mathbf{v}}_v - \vec{\mathbf{v}}_f\right| \mathrm{Re}_v''^{-0.51}\,\mathrm{Pr}_v^{-2/3}, \quad \mathrm{Re}_v'' \leq 50 \\ h'_c &= 0.61 c_{pf} \alpha_v \rho_v \left|\vec{\mathbf{v}}_v - \vec{\mathbf{v}}_f\right| \mathrm{Re}_v''^{-0.41}\,\mathrm{Pr}_v^{-2/3}, \quad \mathrm{Re}_v'' > 50 \end{aligned}, \; \mathrm{Re}_v'' = \frac{\alpha_v \rho_v \left|\vec{\mathbf{v}}_v - \vec{\mathbf{v}}_f\right| D_f}{6\alpha_f \mu_v}. \tag{14}$$

Similarly, for vapor-to-water heat transfer we have, for $\vartheta_v < 0.7$ with vapor as the dispersed phase

$$\dot{Q}_{ws} = n_w \phi_{vw} \pi D_v \lambda_w \left(2 + 0.6 \mathrm{Re}_w^{1/2} \mathrm{Pr}_w^{1/3} \right) (T_s - T_w),$$
$$\dot{Q}_{vs} = 2 n_w \phi_{vw} \pi D_v \lambda_v (T_s - T_v), \tag{15}$$

while for $\vartheta_v \geq 0.7$, with liquid as the dispersed phase

$$\dot{Q}_{vs} = n_w \phi_{wv} \pi D_w \lambda_v \left(2 + 0.6 \mathrm{Re}_v^{1/2} \mathrm{Pr}_v^{1/3} \right) (T_s - T_v),$$
$$\dot{Q}_{ws} = 2 n_w \phi_{wv} \pi D_w \lambda_w (T_s - T_w). \tag{16}$$

3. Description of the Premixing Experiments

3.1 Isothermal experiments at the University of Oxford

Isothermal premixing experiments have been performed at the University of Oxford [3], in which a two-dimensional array of 6 mm diameter balls, initially held at predetermined spacing by perforated belts, was projected downwards into a tank of water 475 mm wide, 925 mm deep and 7.8 mm thick. The planar two-dimensional geometry provided a good visualization of conditions within the jet. Most of the experiments were performed with stainless steel balls and a few with aluminium balls. In the experiment considered stainless steel balls were projected in a jet 10 columns (87 mm) wide and entered the water at a velocity of 1.7 m/s and a phase presence probability of 0.10.

3.2 Experiments at the QUEOS facility

In these QUEOS experiments [4] up to 20 kg of spheres, made of steel, zirconia or molybdenum, were heated to temperatures up to 2300°C and discharged into 0.5 m^3 of saturated water (Table 1). The water level in the vessel with an inner cross section of 70 cm x 70 cm and a height of 138 cm was 100 cm. In all experiments the jet diameter was 9 cm and the spheres entered the water at a velocity of 5.12 m/s and a phase presence probability of 0.17. The following QUEOS experiments were simulated:

Experiment	Material	Diameter [mm]	Mass [kg]	Volume [cm3]	Number of spheres	Temperature [K]
Q01	steel	4.7	20	4440	46000	300
Q02	steel	4.7	10	2220	23000	300
Q05	ZrO_2	5.0	7.0	1830	18000	300
Q09	ZrO_2	5.0	7.0	1880	18000	1300
Q06	ZrO_2	10.0	7.0	1900	2340	300
Q07	ZrO_2	10.0	7.0	1900	2340	1300
Q08	Mo	4.2	10	1800	24000	300
Q04	Mo	4.2	10	1800	24000	1300
Q11	Mo	4.2	5.7	1025	13700	1800
Q12	Mo	4.2	6.9	1183	16600	2300

Table 1: Conditions of simulated QUEOS premixing experiments.

4. Results of the Simulation

4.1 Isothermal experiments at the University of Oxford

The simulation of the Gilbertson experiment [3] has been performed in the rectangular coordinate system on meshes 14x37, 26x72 and 50x142 grid points. Since the analysis of video

data from the experiments showed that the drag coefficient was 0.76, this increase above the standard value 0.44 presumably being caused by the presence of the tank walls, the correct higher drag coefficient was taken for the calculations. The results of the simulations are presented on Fig. 2 where they are compared to experimental data and also to the first order accurate upwind calculations. The convergence analysis showed that the ESE results calculated with the second order accurate high-resolution method don't depend much on the grid density. On the largest mesh 50x142 grid points also the upwind method produces nearly perfect results.

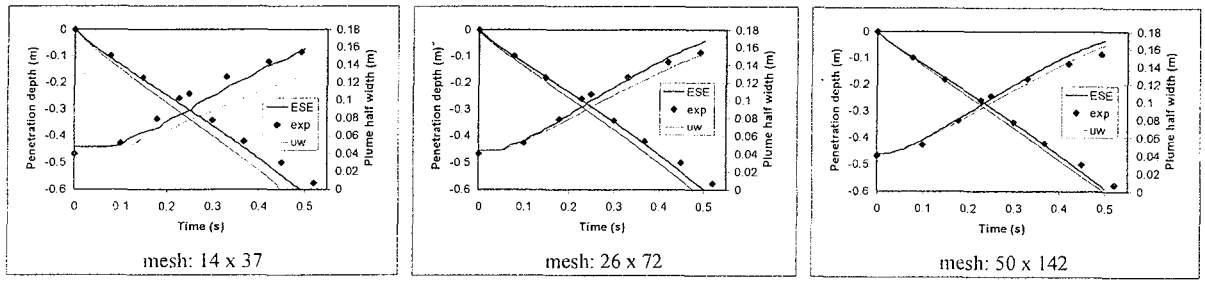

Figure 2: Comparison of Penetration depth and Plume half width between ESE, experiment and upwind method calculations.

4.2 Experiments at the QUEOS facility

The simulation of the QUEOS experiments has been performed in the cylindrical coordinate system on a mesh 41x120 grid points. For the cold experiments the penetration depth and the plume half width have been compared to experimental data and to the first order accurate upwind calculation (Fig. 3), whereas for the hot experiments also the comparison of the steam flow rate and the total steam volume is presented (Fig. 4, 5).

4.2.1 Cold experiments

The first spheres touch the water surface with a velocity of about 5 m/s and are decelerated to approximately 3 m/s. The succeeding spheres push the spheres which are already in the water sideways and downward, thereby opening a gas channel twice as wide as the original diameter of the sphere jet. Since the later spheres fall within the gas channel they still accelerate and meet the sphere front at a higher velocity and the front velocity increases again.

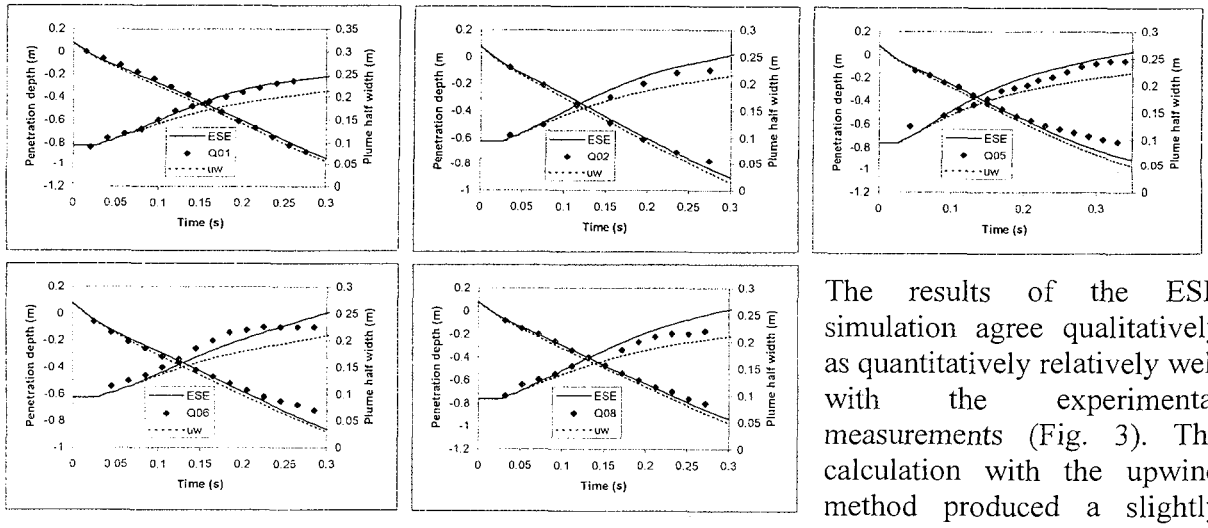

Figure 3: Comparison of Penetration depth and Plume half width between ESE, experiment and upwind method calculations.

The results of the ESE simulation agree qualitatively as quantitatively relatively well with the experimental measurements (Fig. 3). The calculation with the upwind method produced a slightly faster front propagation as a consequence of the artificial numerical diffusion and less

spreading since the inverted mushroom structure did not develop completely. The described decelerating-accelerating-decelerating front velocity behavior was reproduced only with the ESE simulation.

4.2.2 Hot experiments

In the tests with hot spheres an effect occurs which breaks up the front of the sphere cloud. While the spheres are resting upon the middle valve in the radiation furnace the pressure increases due to the heat up of the gas in the closed space between the upper and the lower valve. When the lower valve is opened a gas burst, which disturbs the water surface, can be observed. When the middle valve opens, there is still some overpressure above the spheres and gas is forced through the spheres accelerating the front spheres. In these tests always a small number of spheres is ahead the bulk. Therefore a pressure relief valve was installed above the middle sliding door which opens together with the lower sliding door valve. This reduced this effect somewhat (starting with Q11).

The comparison of the penetration depth and the plume half width between the second order accurate ESE simulation, the experiment measurements and the simulation performed with the first order accurate upwind method is presented on Fig. 4. The results of the ESE simulation are in relatively good agreement with the experimental data.

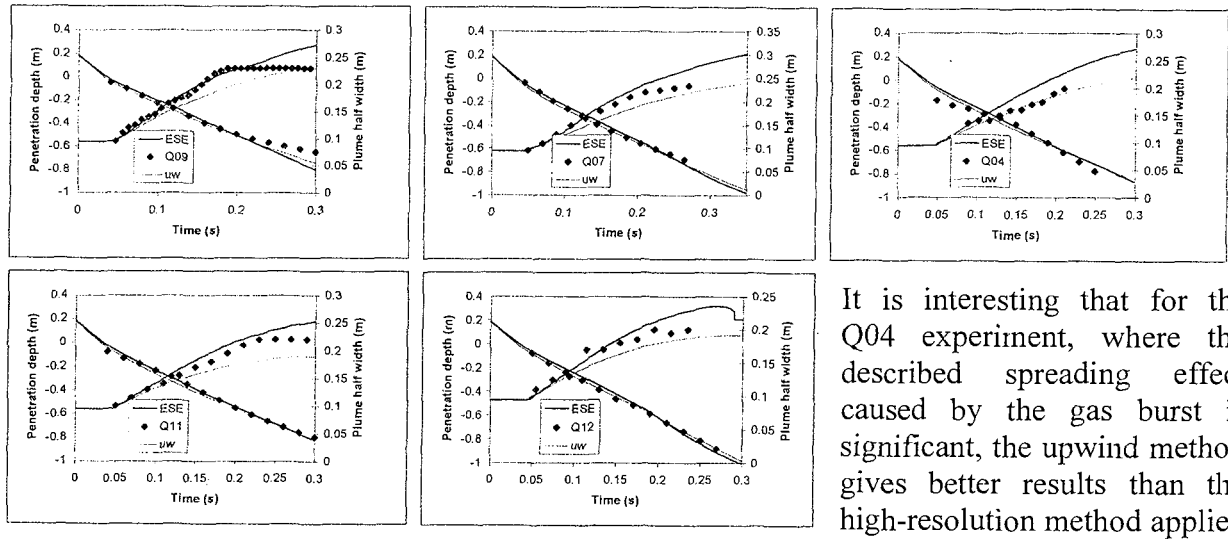

Figure4: Comparison of Penetration depth and Plume half width between ESE, experiment and upwind method calculations.

It is interesting that for the Q04 experiment, where the described spreading effect caused by the gas burst is significant, the upwind method gives better results than the high-resolution method applied in the ESE code. The reason may be that the numerical diffusion of the first order accurate upwind method produces similar spreading of the spheres than the not modeled gas burst.

On Fig. 5 the comparison of the steam flow rate and the total steam volume between the ESE simulation, the experiment and the simulation performed with the upwind method is presented. The results of the ESE simulation show qualitatively the correct dynamics of the steam production, but there are some deviations in the absolute value of the steam flow rate. In all simulation the steam flow rate is zero till the first hot spheres enter the water, whereas in the experiments there is significant steam flow also before. The reason is the heating of the steam atmosphere above the water during the hot spheres free fall, which was not simulated, and maybe also little evaporation of the water surface due to radiation. Radiation was taken into account in ESE only with an intracell model not considering the intercell radiation influence. In the first part of the premixing phase the upwind method and the high-resolution method applied in ESE give similar results for the steam flow rate, whereas in the second part the steam generation is higher for the upwind method. The main reason for that behavior is the high

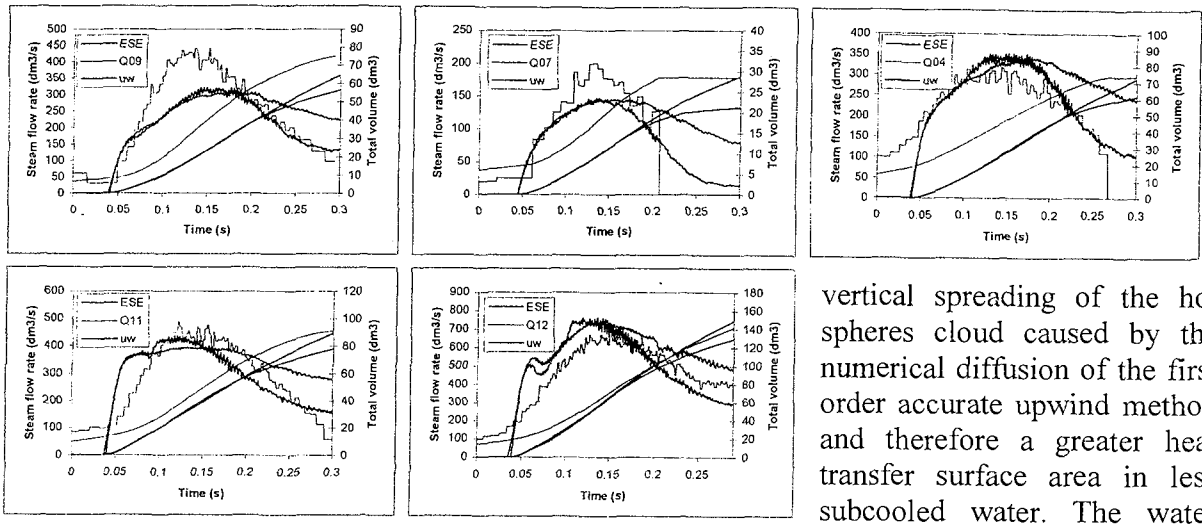

Figure 5: Comparison of Steam flow rate and Total steam volume between ESE, experiment and upwind method calculations.

vertical spreading of the hot spheres cloud caused by the numerical diffusion of the first order accurate upwind method and therefore a greater heat transfer surface area in less subcooled water. The water subcooling is caused by the hydrostatic pressure and the pressure increase due to evaporation.

5. Conclusions

ESE the general second order accurate two-dimensional compressible multiphase flow computer code has been validated against a number of premixing experiments performed at the University of Oxford and at the QUEOS facility at Forschungszentrum Karlsruhe. In these premixing experiments different jets of spheres were injected in a water pool. The ESE validation plan was carefully chosen, starting from very simple, well-defined problems, and gradually working up to more complicated ones. The hydrodynamic part of ESE could be tested separately using results from the Gilbertson experiments performed in rectangular geometry and the isothermal QUEOS experiments performed in axial-symmetric cylindrical geometry. The complete behavior of ESE was validated using results from the hot integral QUEOS experiments. To get a better understanding of ESE's numerical behavior all calculations were performed, beside using ESE's second order accurate high-resolution method, also using a first order accurate upwind method.

Most of the ESE results agree qualitatively as quantitatively reasonably well with experimental data and they are in general better than the results obtained with the first order accurate upwind calculation. The greatest deviation between the simulation and the experimental measurements appeared for the steam flow rate most likely because of the unrealistic determined initial conditions (gas burst spreading, ...) in combination with uncomplete modeling (steam atmosphere heating, intercell radiation, ...).

6. References

[1] M. Leskovar, J. Marn: *Simulation of High Temperature Molten Fuel Coolant Mixing.* ASME International Mechanical Engineering Congress, Atlanta, Proceedings (1996), pp. 99-101.

[2] W.H. Amarasooriya, T.G. Theofanous: *Premixing of Steam Explosions: A Three-Fluid Model.* Nucl. Eng.& Design, 126, 23-39, (1991).

[3] M.A. Gilbertson, D.B.R. Kenning, D.F. Fletcher: *Small-scale Coarse Mixing Experiments: Problems of Comparison with Multiphase Flow models.* Proc. Int. Conf. on New Trends in Nuclear System Thermohydraulics (1994), Vol.2, pp. 247-255.

[4] L. Meyer, G. Schumacher: QUEOS, a Simulation-Experiment of the Premixing Phase of a Steam Explosion with Hot Spheres in Water, Base Case Experiments. FZKA Report 5612, Forschungszentrum Karlsruhe, (1996).